

Cite this: *Dalton Trans.*, 2019, **48**, 3825

Received 14th December 2018,

Accepted 14th February 2019

DOI: 10.1039/c8dt04928a

rsc.li/dalton

Bi-stable spin-crossover characteristics of a highly distorted $[\text{Fe}(\text{1-BPP-COOC}_2\text{H}_5)_2](\text{ClO}_4)_2 \cdot \text{CH}_3\text{CN}$ complex†

Kuppusamy Senthil Kumar,^a Benoît Heinrich,^a Sergi Vela,^b Eufemio Moreno-Pineda,^c Corinne Bailly^d and Mario Ruben^{a,c}

A highly distorted high spin Fe(II)-complex, $[\text{Fe}(\text{1-BPP-COOC}_2\text{H}_5)_2](\text{ClO}_4)_2 \cdot \text{CH}_3\text{CN}$, with a *trans*-N(pyridine)–Fe–N(pyridine) angle (ϕ) of 158.83(17)° showed lattice solvent dependent bi-stable spin-state switching characteristics with $T_{1/2} = \text{ca. } 233 \text{ K}$ and a high thermal hysteresis width (ΔT) of 101 K, for the first cooling and heating cycle, unprecedented for the $[\text{Fe}(\text{BPP})_2]^{2+}$ series of complexes; the results presented in this study are fundamentally important and have implications towards the realization of device architectures based on bi-stable SCO complexes.

Mononuclear Fe(II)-complexes capable of undergoing spin-crossover (SCO) from the diamagnetic low-spin (LS) to paramagnetic high-spin (HS) state are suitable candidates for the development of molecule-based memory and switching architectures.^{1–6} To be optimal candidates for applications, SCO systems should show abrupt and hysteretic SCO.^{1,3,5,7,8} The complexes showing such a cooperative and hysteretic spin state switching are termed bi-stable, due to the presence of a hysteresis loop conferring memory effect.⁹ In this context, several mononuclear and polymeric SCO complexes are reported to exhibit spin-state switching with a technologically relevant thermal hysteresis width, $\Delta T \geq 45 \text{ K}$.¹⁰ Notably absent in the list of mononuclear Fe(II)-complexes showing $\Delta T \geq 45 \text{ K}$

are prototypical $[\text{Fe}(\text{1-bpp-R})_2](\text{X})_2$, R = functional groups^{11–15} and X = BF_4^- , ClO_4^- , etc., complexes comprised of the 2,6-di(pyrazol-1-yl)pyridine (1-bpp) family of ligands.^{16,17} This family of complexes is one of the most studied SCO systems due to their propensity to undergo facile spin-state switching owing to the moderate ligand field strength of 1-bpp ligands. The parent $[\text{Fe}(\text{1-bpp-R})_2](\text{BF}_4)_2$ complex, R = H, is reported to show SCO around 259 K with a narrow hysteresis loop of 3 K.¹⁸ Further derivatization of the parent $[\text{Fe}(\text{1-bpp-R})_2](\text{X})_2$ skeleton with various functional groups at the 4-position of the central pyridyl ring resulted in a range of $[\text{Fe}(\text{1-bpp-R})_2](\text{X})_2$ systems exhibiting different switching temperatures and narrow thermal hysteresis widths. Thermal hysteresis widths (ΔT) of 18 K and 35 K reported for the $[\text{Fe}(\text{1-bpp-CH}_3)_2](\text{ClO}_4)_2$ ($T_{1/2} = 184 \text{ K}$)¹⁹ and $[\text{Fe}(\text{1-bpp-CH}_2\text{Br})_2](\text{ClO}_4)_2$ ($T_{1/2} = \text{ca. } 340 \text{ K}$)²⁰ complexes, respectively, are the highest values reported so far.

From the structural view point, the HS $[\text{Fe}(\text{1-bpp-R})_2](\text{X})_2$ complexes are prone to Jahn–Teller (J–T) distortion.²¹ The distorted $[\text{Fe}(\text{1-bpp-R})_2](\text{X})_2$ complexes exhibit (i) a reduced *trans*-N{pyridyl}–Fe–N{pyridyl} angle (ϕ) below 180° (*cf.* Chart 1) and (ii) twisting of the tridentate 1-bpp ligands from the ideal perpendicular arrangement leading to a reduction in the dihedral angle (θ) from its ideal value of 90°.^{16,19,22}

It is observed that $[\text{Fe}(\text{1-bpp-R})_2](\text{X})_2$ complexes exhibiting too pronounced distortions from the ideal octahedral geometry are trapped in the HS state. This is due to the rigid lattice blocking the large structural reorganizations required by the distorted HS system to attain an undistorted/less-distorted LS state. A critical structure–property analysis of $[\text{Fe}(\text{1-bpp})_2](\text{X})_2$ complexes in 2009 led to the conclusion that the complexes featuring the values of $\phi < 172^\circ$ and $\theta < 76^\circ$ are prone to be trapped in the HS state.¹⁶ The recently reported $[\text{Fe}(\text{1-bpp-CH}_3)_2](\text{ClO}_4)_2$ complex by Halcrow and co-workers is a notable exception of this conclusion, and is one of the rare examples of highly distorted $[\text{Fe}(\text{1-bpp-R})_2](\text{X})_2$ complex systems ($\phi = 163.7(2)^\circ$ at 240 K) undergoing SCO.¹⁹

In this contribution, we report abrupt and hysteretic SCO exhibited by a highly distorted $[\text{Fe}(\text{1-bpp-COOC}_2\text{H}_5)_2]$

^aInstitut de Physique et Chimie des Matériaux de Strasbourg (IPCMS), CNRS-Université de Strasbourg, 23, rue du Loess, BP 43, 67034 Strasbourg cedex 2, France. E-mail: senthil.kuppusamy@ipcms.unistra.fr

^bLaboratoire de Chimie Quantique, UMR 7111, CNRS-Université de Strasbourg, 4 rue Blaise Pascal, F-67000 Strasbourg, France

^cInstitute of Nanotechnology, Karlsruhe Institute of Technology (KIT), Hermann-von-Helmholtz-Platz 1, 76344 Eggenstein-Leopoldshafen, Germany. E-mail: mario.ruben@kit.edu

^dService de Radiocristallographie, Fédération de Chimie Le Bel FR2010 CNRS-Université de Strasbourg, 1 rue Blaise Pascal, BP 296/R8, 67008 Strasbourg cedex, France

† Electronic supplementary information (ESI) available: Synthesis and characterization details of the complex, thermogravimetric and differential scanning calorimetric (DSC) analyses, first derivatives of the χT vs. T plots, and crystallographic parameters of the complex. CCDC 1589139. For ESI and crystallographic data in CIF or other electronic format see DOI: 10.1039/c8dt04928a

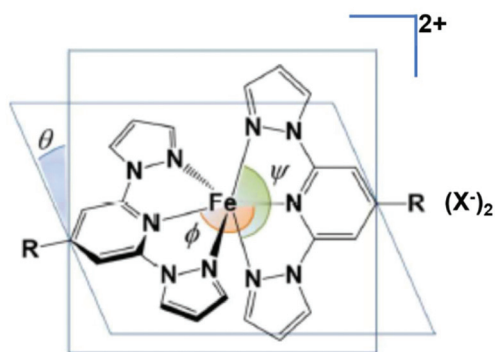


Chart 1 Structural model depicting the angular components of distortion in the HS $[\text{Fe}(\text{1-bpp-R})_2](\text{X})_2$ complexes. The angles ϕ and θ represent the degree of distortion; complexes with an ideal octahedral geometry have $\phi = 180^\circ$ and $\theta = 90^\circ$. The $\text{N}(\text{pyrazole})\text{-Fe-N}(\text{pyrazole})$ clamp angle is represented as ψ .^{19,23} The complex, $[\text{Fe}(\text{1-BPP-COOC}_2\text{H}_5)_2](\text{ClO}_4)_2\cdot\text{CH}_3\text{CN}$, with a co-crystallized CH_3CN solvent and $\text{R} = -\text{COOC}_2\text{H}_5$ and $\text{X} = \text{ClO}_4$ is discussed in this study and is hereafter referred to as complex 1.

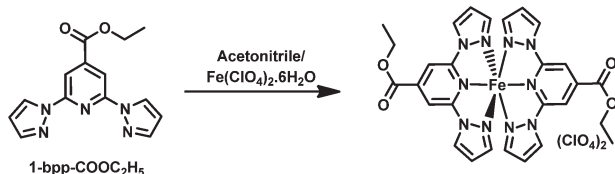
$(\text{ClO}_4)_2\cdot\text{CH}_3\text{CN}$ complex (**1**, *cf.* Chart 1) with the *trans*- $\text{N}\{\text{pyridyl}\}\text{-Fe-N}\{\text{pyridyl}\}$ angle (ϕ) of $158.83(17)^\circ$ and $\theta = 78.74(10)^\circ$.

The synthesis of the ligand $\text{1-bpp-COOC}_2\text{H}_5$ was carried out employing a previously reported procedure.²⁴ The complexation reaction between the ligand and the corresponding $\text{Fe}(\text{II})$ salt was performed using acetonitrile (ACN) as a solvent as depicted in Scheme 1.

Good quality single crystals of complex **1**, suitable for X-ray structure determination, were obtained by slow diffusion of diethyl ether (Et_2O) in the ACN solution of the complex over a period of 2–3 weeks. Once harvested from the mother liquor, the complexes are washed with ether followed by drying under vacuum for 4 h. Elemental and thermogravimetric analyses (TGA) of the samples (*cf.* Fig. S1†) showed no loss of the lattice ACN solvent due to this process.

To gain insights into the SCO characteristics of **1**, standard DC magnetic susceptibility measurements were performed under a 0.1 T applied magnetic field. A scan rate of 1 K min^{-1} was employed and the data were collected in settle mode.³ The complex revealed an abrupt SCO with a *ca.* 101 K hysteresis loop for the first cooling and heating cycle ($T_{1/2\downarrow} = 183 \text{ K}$ and $T_{1/2\uparrow} = 284 \text{ K}$) as shown in Fig. 1.

The second cycle resulted in the reduction of both the χT value and hysteresis width with $T_{1/2\downarrow} = 221 \text{ K}$ and $T_{1/2\uparrow} = 286 \text{ K}$. Interestingly, subsequent cycles 3 ($T_{1/2\downarrow} = 210 \text{ K}$ and $T_{1/2\uparrow} = 289 \text{ K}$)



Scheme 1 Synthesis of complex 1.

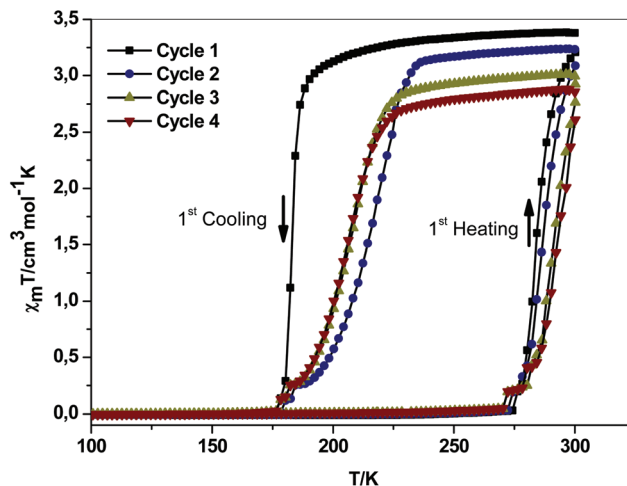


Fig. 1 $\chi_m T$ vs. T plot of complex **1**. See Table S1† for the collection of parameters associated with the spin-state switching.

and 4 ($T_{1/2\downarrow} = 207 \text{ K}$ and $T_{1/2\uparrow} = 294 \text{ K}$) resulted in an increased hysteresis width as depicted in Fig. 1 (see Table S1 and Fig. S2† for further details).

To understand the role of the lattice ACN solvent in effecting the bi-stable SCO of **1**, SQUID measurements were performed by heating a freshly/newly prepared sample up to 400 K, the temperature just above the release temperature of the co-crystallized ACN (measured at 398 K by TGA, *cf.* Fig. S1†). The first cool–heat cycle in the presence of all the lattice solvent showed bi-stable SCO with $T_{1/2} = 233 \text{ K}$ and $\Delta T = 100 \text{ K}$ (*cf.* Fig. S3†), reproducing the spin-state switching characteristics depicted in Fig. 1. In the second cooling step, HS to LS switching occurred at a higher temperature, relative to the first cooling branch, with $T_{1/2} = 258 \text{ K}$ (*cf.* Fig. S3b†). Subsequent heating (second heating) of the sample resulted in the occurrence of gradual and incomplete SCO ($\chi_m T = ca. 0.84 \text{ cm}^3 \text{ mol}^{-1} \text{ K}$, 400 K) with the dominant remnant LS fraction. The subsequent cooling–heating cycle (third cycle) resulted in stabilized SCO behaviour closely resembling that of the second heating branch. At this stage, the lattice solvent was totally removed as demonstrated by the TGA curve of the sample recovered from the third SQUID cycle (*cf.* Fig. S3 and S4†). Consistently, the SCO transition peak vanished in DSC experiments (Fig. S5†) and a completely different crystal structure was found by powder X-ray diffraction (PXRD) for the solvent-free complex (*cf.* Fig. S6†). Interestingly, TGA measurements of complex **1** obtained after four cool–heat cycles, from differential scanning calorimetry (DSC) measurements (*vide infra*), revealed a gradual lattice solvent release starting around 350 K as depicted in Fig. S4.† PXRD measurements of the same sample have shown a structural modification or phase transition in comparison with the pristine complex **1** (*cf.* Fig. S6†).

In the first SQUID experiment conducted up to 300 K (Fig. 1), the temperature was constantly far below that of solvent release, and a drift of the SCO behaviour nevertheless

occurred. As a matter of fact, the same crystal structure could give such divergent SCO behaviours if the multiple cycling altered the quality of crystallization. This is just what was found by Real and co-workers, who reported on a cyanide-bridged Fe(II)–Ag(I) bimetallic complex that repeated heating–cooling cycles resulted in the cracking of the crystals to a fine microcrystalline powder and the stabilization of the HS state without affecting the thermal hysteresis width and location.²⁵ Another study reported the disintegration of crystals of a mononuclear Fe(II)–SCO complex, [Fe(DAPP)(abpt)](ClO₄)₂, into smaller crystallites upon thermal cycling attributed to a “self-grinding effect” mediated by spin-state switching.²⁶ The crystal size reduction of [Fe(DAPP)(abpt)](ClO₄)₂ also resulted in an increase and decrease in the $T_{1/2}$ and $\chi_m T$ values, respectively, coinciding with the magnetic characteristics of complex **1** presented in Fig. 1. Thus, the observed χT value reduction of **1** upon repeated cycling is most probably due to the cracking of the crystalline complex (self-grinding) accompanied by concomitant lattice solvent release and structural modifications or phase transition.

Differential scanning calorimetry (DSC) measurements performed on the crystalline sample of **1** at two different scan rates of 2 K min^{−1} and 8 K min^{−1} revealed the scan rate dependence of ΔT as depicted in Fig. 2 and Table S2.† Four cool–heat cycles were performed at each scan rate and the results reproduced the trends observed in the $\chi_m T$ vs. T plots shown in Fig. 1.

Relatively sharp transition peaks were observed in the first cool–heat cycle, whereas more broadened peaks were observed in the subsequent cool–heat cycles, which reproduces the evolution of the SCO steepness in the SQUID experiment (Fig. 1). The $T_{1/2} = 231$ K and $\Delta T = 104$ K obtained from the DSC measurements performed at 2 K min^{−1} (cycle 1) are also in close agreement with the SCO parameters ($T_{1/2} = 233$ K and $\Delta T = 101$ K) obtained from the magnetic measurements (cycle 1); see Tables S1 and S2† for more details. The experimentally deduced enthalpy and entropy values of 7.15 kJ mol^{−1} and 32.35 J K^{−1} mol^{−1} (scan rate = 2 K min^{−1}, cycle 1), respectively, are in the range reported for the Fe(II)–SCO complexes.²⁷ The

entropy values are greater than the value of 13.4 J K^{−1} mol^{−1} expected solely on the spin multiplicity change occurring upon SCO; the excess entropy would be ascribed to the differing intramolecular vibrational modes coupled with the LS and HS spin-states of **1**.²⁸

The more broadened nature of the transition peaks observed upon repeated thermal cycling indicates the less cooperative nature of the SCO agreeing with the $\chi_m T$ vs. T plots shown in Fig. 1.

The fitting of the χT curve obtained in the first cycle (cf Fig. S7†), using the Slichter–Drickamer (SD) model,²⁹ yielded $\Delta H = 8.62$ kJ mol^{−1}, $\Delta S = 34.0$ J K^{−1} mol^{−1} and $\Gamma = 7.0$ kJ mol^{−1}. In turn, the second cycle (cf Fig. S8†) yielded $\Delta H = 7.12$ kJ mol^{−1}, $\Delta S = 27.4$ J K^{−1} mol^{−1} and $\Gamma = 6.3$ kJ mol^{−1}. It thus follows that the ratio of ΔH and ΔS between the first and second cycles is, in both cases, *ca.* 81%. A comparison between the experimental and fitted curves is offered in the ESI; see Fig. S7 and S8.† Whereas the first cycle could be fitted very satisfactorily, the second cycle could not be fitted with good quality. The reason is the combination of (i) the gradual decrease of χT in the cooling process and (ii) such a wide hysteresis loop. The former requires a small Γ whereas the latter requires a large Γ . The best fit was found at $\Gamma = 6.3$ kJ mol^{−1}, but its overall quality is not excellent (see Fig. S8†). A cooperativity factor (C)³⁰ of 3.61 (*cf.* Table 1) was obtained at $T_{1/2} = 233$ K indicating the bi-stable nature of the SCO.

To get insights into various factors contributing to the abrupt and hysteretic SCO of **1**, a crystallographic analysis of the complex was carried out. The complex crystallized in the triclinic $P\bar{1}$ space group with two complex and two solvent molecules constituting the unit cell; see Fig. 3 for the structure of the complex cation. At 253 K, the complex is in its HS state as inferred from the structural parameters depicted in Table 2, which agrees well with the χT vs. T plots described above.

The crystal structure of the complex clearly reveals the distorted nature of the octahedral coordination environment as implied by the *trans*-N{pyridyl}–Fe–N{pyridyl} angle (ϕ) of 158.83(17)° and the dihedral twist angle (θ) = 78.74(10)°. The observed clamp angles (ψ) of 146.10(17)° and 145.29(17)°, the

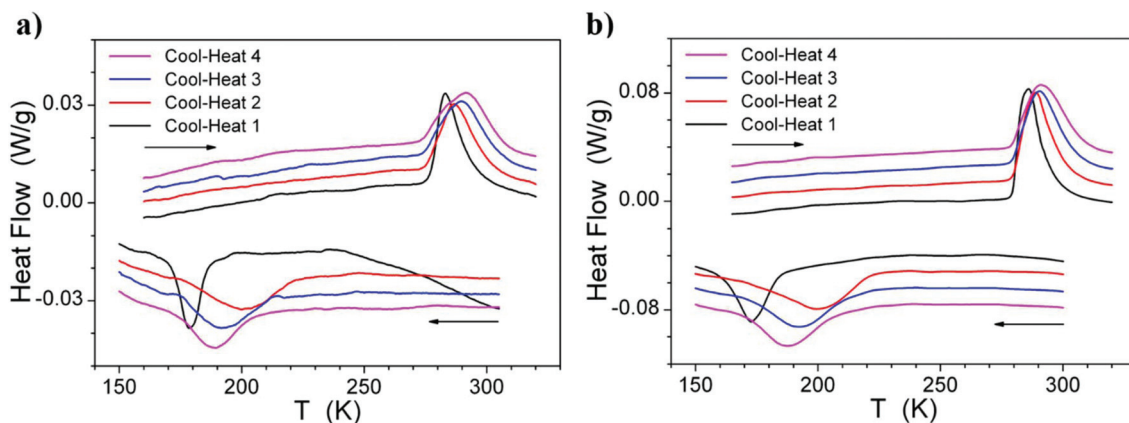


Fig. 2 DSC analysis of complex **1** at (a) 2 K min^{−1} and (b) 8 K min^{−1} scan rates (endotherm, top). Four cycles were performed at each scan rate.

Table 1 Thermodynamic parameters involved in the SCO of the complex

DSC					SQUID		SD model			
SR ^a	T _{1/2} ^b	ΔT ^b	ΔH ^c	ΔS ^d	T _{1/2} ^b	ΔT ^b	ΔH ^c	ΔS ^d	Γ ^c	C = Γ/RT _{1/2}
2 ^e	231	104	7.15	32.35	233	101	8.62	34.0	7.0	3.61
8 ^e	229.5	113	6.3	28.9						

^a In K min⁻¹. ^b In K. ^c In kJ mol⁻¹. ^d In J K⁻¹ mol⁻¹. ^e From the 1st cool-heat cycle.

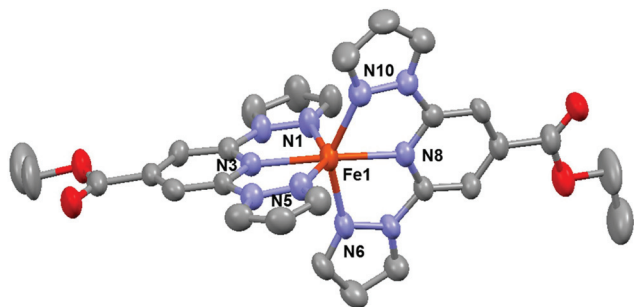


Fig. 3 View of the complex di-cation in the crystal structure of **1**. Displacement ellipsoids are at the 50% level. Symmetry transformation used to generate equivalent atoms $-X$, $-Y$, and $-Z$.

Table 2 Selected bond lengths (Å), angles, and distortion indices (°) of complex **1**

Parameter	Value	Parameter	Value
T/K	253	rFe–N (average)	2.16(2)
rFe ₁ –N ₁ (pyrazolyl)	2.184(5)	N ₃ –Fe ₁ –N ₈ (ϕ)	158.83(17)
rFe ₁ –N ₃ (pyridyl)	2.134(4)	N ₆ –Fe ₁ –N ₁₀ (ψ)	146.10(17)
rFe ₁ –N ₅ (pyrazolyl)	2.161(5)	N ₁ –Fe ₁ –N ₅ (ψ)	145.29(17)
rFe ₁ –N ₆ (pyrazolyl)	2.183(5)	Σ	159.71
rFe ₁ –N ₈ (pyridyl)	2.136(4)	θ	78.74(10)
Fe ₁ –N ₁₀ (pyrazolyl)	2.174(5)	α	73.427(5)

average Fe–N bond length = 2.16(2) Å and the distortion index (Σ) = 159.71 clearly indicate the HS state of the complex at 253 K. The average value of four *cis*-N{pyridyl}–Fe–N{pyrazole} angles (α) = 73.427(5)° exhibited by **1** is a testimony of reduced bite angles exhibited by 1-bpp-R ligands.¹⁶

The crystal packing of **1** is best described as a zig-zag arrangement of the complex cations along the crystallographic axis *c* (cf. Fig. 4a) mediated by short contacts involving acetonitrile solvent molecules and complex cations and counter anions. No direct interactions between the complex cations were observed. The pseudo-1D-chain like molecular organization stacks along the crystallographic axis *b*. Extensive intermolecular interactions among the complex cation, counter anion, and acetonitrile solvent are observed in the (*a*, *c*) plane of the unit cell as depicted in Fig. 4b.

The short contacts involve: (i) the hydrogen atom of the pyrazole moiety of the complex cation and the oxygen atom of the solvent (H15–O7, *d* = 2.43 Å), (ii) the oxygen atom of the carbonyl moiety of the complex cation and the hydrogen atom of the

solvent (O1–H29B, *d* = 2.53 Å), (iii) the hydrogen atom of the pyrazole moiety and the oxygen atom of the counter anion (H9–O9, *d* = 2.59 Å), (iv) the oxygen atom of the counter anion and the hydrogen atom of the solvent (O5–H29C, *d* = 2.42 Å), and (v) the carbon atom of the complex cation and the oxygen atom of the counter anion (C12–O5, *d* = 3.017(8) Å). Our attempts to determine the structure of the LS complex were not fruitful due to the fast disintegration of the crystal upon cooling below the SCO temperature.

The present contribution originated due to our attempts to study self-assembly dependent SCO in linear alkyl-chain tethered [Fe(1-bpp)₂](X)₂ complexes anchored on a graphene surface. During our study, Halcrow and co-workers reported the SCO characteristics of [Fe(1-bpp-COOR)₂] complexes with R = C₁₈ and C₁₂.³¹ Recently, Coronado and co-workers reported the magnetic characteristics of the [Fe(1-bpp-COOC₂H₅)₂](ClO₄)₂·CH₃COCH₃ complex showing the first-order spin-state switching from the LS to HS state at *ca.* 330 K. However, the complex remained at the HS state during the cooling cycle, which was attributed to the loss of the lattice solvent and subsequent kinetic trapping in the HS state.³² In the present case, complex **1** underwent lattice solvent dependent bi-stable SCO and the complete loss of the ACN solvent trapped the system predominantly in the LS state. In another study, Rigamonti and co-workers reported a lattice-solvent-free HS [Fe(1-bpp-COOCH₃)₂](ClO₄)₂ complex featuring a pronounced distortion of the *trans*-N{pyridyl}–Fe–N{pyridyl} angle (ϕ) = 158.77(5)°.²³ Such strong distortion and the direct intermolecular interactions operating between the [Fe(1-bpp-COOCH₃)₂] complex cations packed in a so called “terpyridine embrace lattice” were attributed to the trapping of the system in its HS state. Interestingly, complex **1** shows a similar distorted coordination geometry to the previously reported [Fe(1-bpp-COOCH₃)₂] complex, and yet shows SCO. Remarkably, complex **1** reported in this study has shown a reduced dihedral twist angle (θ) = 78.74(10)° than the [Fe(1-bpp-COOCH₃)₂](ClO₄)₂ complex (θ = 80.738(12)°) reported by Rigamonti and co-workers indicating a more distorted nature of **1** in terms of both shape and size.²³

The bistability displayed by **1** in this manuscript has important consequences towards the understanding of hysteretic SCO in the [Fe(1-bpp-R)₂](X)₂ family of complexes. It is a fact that distorted HS complexes are more likely to remain in the HS state than non-distorted ones.¹⁶ This is due to the molecules being kinetically trapped.³³ For most of the systems based on [Fe(1-bpp-R)₂](X)₂, such behaviour manifests itself in the blockade of the HS state for the entire range of tempera-

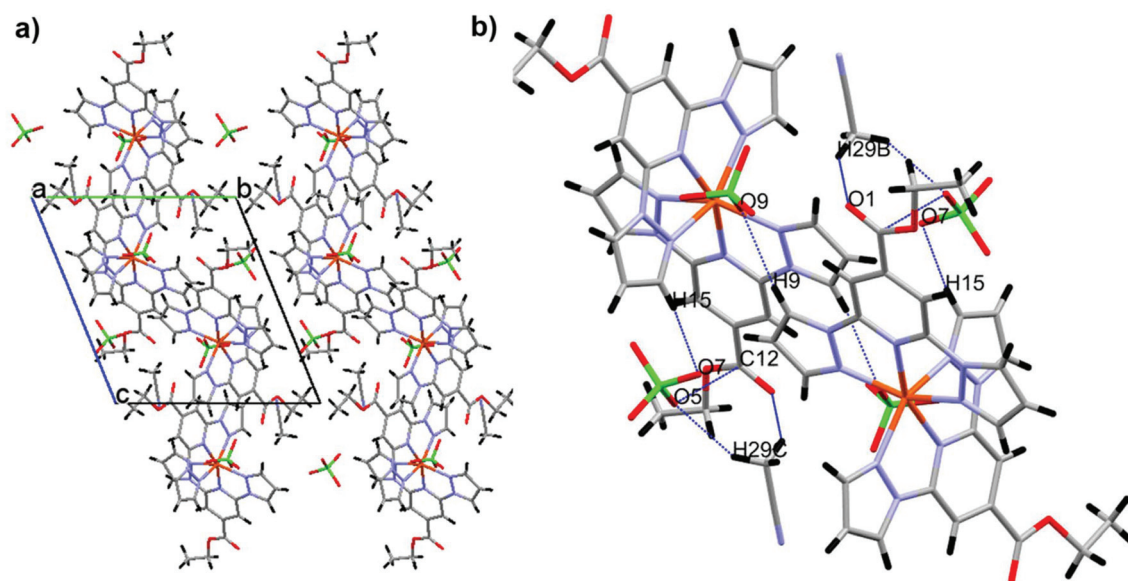


Fig. 4 (a) Crystal packing of **1** and (b) intermolecular contacts associated among the constituents of the unit cell.

tures. This is indeed the expected behavior since, once the molecule gets trapped at a given temperature, further cooling implies that the vibrational energy diminishes and, with it, the chances to escape from the kinetic trapping. In contrast, the distortion of the HS structure in complex **1** gives rise to a hysteresis loop. Notice that a hysteresis loop is also a form of kinetic trapping, but limited to a range of temperatures. Therefore, complex **1** is an example of a $[\text{Fe}(\text{1-bpp-R})_2](\text{X})_2$ complex with insufficient steric constraint to block its HS state for the entire range of temperatures, thus leading to hysteresis. This is probably due to the combination of (i) a distorted geometry, and (ii) the presence of lattice solvent molecules. The latter seems crucial to provide enough free volume for the distorted SCO molecules to switch, as supported by the gradual and incomplete SCO encountered after the release of the co-crystallized solvent. This shed light on literature findings, such as the solvent-free $[\text{Fe}(\text{1-bpp-COOC}_2\text{H}_5)_2](\text{ClO}_4)_2$ remaining kinetically trapped in its HS state²³ and $[\text{Fe}(\text{1-bpp-COOC}_2\text{H}_5)_2](\text{ClO}_4)_2 \cdot \text{CH}_3\text{COCH}_3$ showing abrupt LS to HS switching.³²

In the thermodynamic mean-field models, cooperativity refers to the non-linear part of the equation describing the evolution of the Gibbs energy as a function of the HS molar fraction. In the absence of cooperativity, for instance in the solution phase, the energy required to switch two SCO molecules is exactly twice that of switching one (*i.e.* linear dependence). In cooperative systems, the second molecule is somehow affected by the first switch; therefore it requires a different amount of energy (*i.e.* non-linear dependence). In the well-known Slichter–Drickamer model (SD), the non-linear term is described with the very simple expression $\gamma_{\text{HS}}(1 - \gamma_{\text{HS}})\Gamma$.²⁹ The success of the SD model relies on its simplicity (notice that this term is no more than a parabola centred at $\gamma_{\text{HS}} = 0.5$) and this is usually sufficient to fit most of the experi-

mental SCO curves, as we did above. However, the SD model and, in general, any thermodynamic model, does not clarify the atomistic origin of cooperativity. A common practice is to associate it with the amount of intermolecular contacts in a crystal. The reason for doing so is that intermolecular interactions are the only way to generate sufficient non-linear energy dependence. In other words, cooperativity requires intermolecular interactions.³⁴ However, it is impossible to ascertain which intermolecular contacts contribute to such non-linear behaviour. Clearly, not all of them do, since it has been proven that cooperativity is not necessarily proportional to the amount of intermolecular interactions.³⁵ Having this in mind, we are reluctant to associate the hysteretic behaviour of **1** with any structural feature. However, as we discussed above, this manuscript suggests that molecular distortion can contribute towards generating a hysteretic spin-state switching in molecular SCO complexes, at least for $[\text{Fe}(\text{1-bpp})_2]^{2+}$ systems.

To summarise, we report a rare example of a molecular Fe(II) complex, $[\text{Fe}(\text{1-bpp-COOC}_2\text{H}_5)_2](\text{ClO}_4)_2 \cdot \text{CH}_3\text{CN}$, showing abrupt and hysteretic SCO attributed to the presence of acetonitrile lattice-solvent molecules and a distorted molecular geometry. The serendipitous results observed in this study emphasize once again the sensitive nature of the SCO transition, even to the slightest of the changes in terms of the molecular structure, lattice-solvent and intermolecular interactions. The results presented in the present study could be a stepping stone towards the realization of bi-stable SCO systems for practical applications.

Conflicts of interest

There are no conflicts of interest to declare.

Acknowledgements

Grant Agency Innovation Fondation pour la Recherche en Chimie (FRC)-Strasbourg is acknowledged for the financial support for the project Self-assembly of spin crossover (SCO) complexes on graphene. M. R. thanks the DFG priority program 1928 "COORNETS" for generous support.

References

- 1 B. Weber, W. Bauer and J. Obel, *Angew. Chem., Int. Ed.*, 2008, **47**, 10098–10101.
- 2 K. Senthil Kumar and M. Ruben, *Coord. Chem. Rev.*, 2017, **346**, 176–205.
- 3 S. Brooker, *Chem. Soc. Rev.*, 2015, **44**, 2880–2892.
- 4 E. Burzurí, A. García-Fuente, V. García-Suárez, K. Senthil Kumar, M. Ruben, J. Ferrer and H. S. J. van der Zant, *Nanoscale*, 2018, **10**, 7905–7911.
- 5 J.-F. Létard, P. Guionneau, E. Codjovi, O. Lavastre, G. Bravic, D. Chasseau and O. Kahn, *J. Am. Chem. Soc.*, 1997, **119**, 10861–10862.
- 6 M. A. Halcrow, *Spin-crossover materials: properties and applications*, J. Wiley and Sons, Inc., Chichester, 2013.
- 7 E. Tailleur, M. Marchivie, N. Daro, G. Chastanet and P. Guionneau, *Chem. Commun.*, 2017, **53**, 4763–4766.
- 8 H. Hagiwara, T. Masuda, T. Ohno, M. Suzuki, T. Udagawa and K. Murai, *Cryst. Growth Des.*, 2017, **17**, 6006–6019.
- 9 O. Kahn, J. Kröber and C. Jay, *Adv. Mater.*, 1992, **4**, 718–728.
- 10 M. A. Halcrow, *Chem. Lett.*, 2014, **43**, 1178–1188.
- 11 I. Šalitroš, N. T. Madhu, R. Boča, J. Pavlik and M. Ruben, *Monatsh. Chem. - Chem. Mon.*, 2009, **140**, 695–733.
- 12 N. T. Madhu, I. Salitros, F. Schramm, S. Klyatskaya, O. Fuhr and M. Ruben, *C. R. Chim.*, 2008, **11**, 1166–1174.
- 13 K. Takahashi, Y. Hasegawa, R. Sakamoto, M. Nishikawa, S. Kume, E. Nishibori and H. Nishihara, *Inorg. Chem.*, 2012, **51**, 5188–5198.
- 14 K. S. Kumar, I. Šalitroš, E. Moreno-Pineda and M. Ruben, *Dalton Trans.*, 2017, **46**, 9765–9768.
- 15 R. González-Prieto, B. Fleury, F. Schramm, G. Zoppellaro, R. Chandrasekar, O. Fuhr, S. Lebedkin, M. Kappes and M. Ruben, *Dalton Trans.*, 2011, **40**, 7564.
- 16 M. A. Halcrow, *Coord. Chem. Rev.*, 2009, **253**, 2493–2514.
- 17 M. A. Halcrow, *Coord. Chem. Rev.*, 2005, **249**, 2880–2908.
- 18 J. M. Holland, C. A. Kilner, M. Thornton-Pett, M. A. Halcrow, J. A. McAllister and Z. Lu, *Chem. Commun.*, 2001, 577–578.
- 19 L. J. Kershaw Cook, F. L. Thorp-Greenwood, T. P. Comyn, O. Cespedes, G. Chastanet and M. A. Halcrow, *Inorg. Chem.*, 2015, **54**, 6319–6330.
- 20 H. Douib, L. Cornet, J. F. Gonzalez, E. Trzop, V. Dorcet, A. Gouasmia, L. Ouahab, O. Cadour and F. Pointillart, *Eur. J. Inorg. Chem.*, 2018, **2018**, 4452–4457.
- 21 M. A. Halcrow, *Chem. Soc. Rev.*, 2013, **42**, 1784–1795.
- 22 L. J. Kershaw Cook, R. Mohammed, G. Sherborne, T. D. Roberts, S. Alvarez and M. A. Halcrow, *Coord. Chem. Rev.*, 2015, **289–290**, 2–12.
- 23 N. Bridonneau, L. Rigamonti, G. Poneti, D. Pinkowicz, A. Forni and A. Cornia, *Dalton Trans.*, 2017, **46**, 4075–4085.
- 24 T. Vermonden, D. Branowska, A. T. Marcelis and E. J. Sudhölter, *Tetrahedron*, 2003, **59**, 5039–5045.
- 25 V. Niel, M. C. Muñoz, A. B. Gaspar, A. Galet, G. Levchenko and J. A. Real, *Chem. - Eur. J.*, 2002, **8**, 2446.
- 26 Y. Miyazaki, T. Nakamoto, S. Ikeuchi, K. Saito, A. Inaba, M. Sorai, T. Tojo, T. Atake, G. S. Matouzenko, S. Zein and S. A. Borshch, *J. Phys. Chem. B*, 2007, **111**, 12508–12517.
- 27 M. Sorai, M. Nakano and Y. Miyazaki, *Chem. Rev.*, 2006, **106**, 976–1031.
- 28 O. Roubeau, M. Castro, R. Burriel, J. G. Haasnoot and J. Reedijk, *J. Phys. Chem. B*, 2011, **115**, 3003–3012.
- 29 C. P. Slichter and H. G. Drickamer, *J. Chem. Phys.*, 1972, **56**, 2142–2160.
- 30 C. Carbonera, C. A. Kilner, J.-F. Létard and M. A. Halcrow, *Dalton Trans.*, 2007, 1284–1292.
- 31 I. Galadzhun, R. Kulmaczewski, O. Cespedes, M. Yamada, N. Yoshinari, T. Konno and M. A. Halcrow, *Inorg. Chem.*, 2018, **57**, 13761–13771.
- 32 V. García-López, M. Palacios-Corella, A. Abhervé, I. Pellicer-Carreño, C. Desplanches, M. Clemente-León and E. Coronado, *Dalton Trans.*, 2018, **47**, 16958–16968.
- 33 S. Vela, J. J. Novoa and J. Ribas-Arino, *Phys. Chem. Chem. Phys.*, 2014, **16**, 27012–27024.
- 34 J. A. Real, A. B. Gaspar, V. Niel and M. C. Muñoz, *Coord. Chem. Rev.*, 2003, **236**, 121–141.
- 35 S. Vela and H. Paulsen, *Dalton Trans.*, 2019, **48**, 1237–1245.